Magnetic properties of sediments within the water-level fluctuation zone of the Three Gorges Reservoir and their response to provenance and hydrodynamic conditions

Ting Chen[1] · Yujie Chen[1] · Xiaofeng Wang[1] · Xingping Wei[1] · Liuliu Feng[1] · Yixuan Wang[1]

Abstract

Purpose Iron-bearing magnetic minerals in the sediments of the water-level fluctuation zone (WLFZ) in large reservoirs play critical roles in the burial and release of organic carbon and pollutants. This study aims to reveal the spatial distribution of magnetic minerals across different elevations and reaches within the WLFZ of the Three Gorges Reservoir (TGR), the largest reservoir in the world, and their links to sediment provenance and hydrodynamic conditions. This study will provide a fundamental basis for future investigations in the roles of magnetic minerals in the circulation processes of pollutants and organic carbon within the WLFZ of fluvial-reservoir systems.

Materials and methods ~300 sediment samples and nearby side-slope soils were collected from various altitudes within the WLFZ at ten different sites of the TGR. The magnetic properties of these sediments and soils were examined using environmental magnetism. Additionally, previously reported data on magnetic properties of suspended sediments from upstream rivers flowing into the TGR were assembled. Nearby side-slope soils and suspended samples were used to represent magnetic properties of potential sources for the sediments within the WLFZ.

Results and discussion Our findings reveal that magnetite/maghemite and hematite particles dominate the sediments within the WLFZ of the TGR. Relatively higher concentration of hematite particles in the upper part (> 165 m) of WLFZ mainly originates from or are nearby side-slope soils, whereas higher concentration of magnetite/maghemite particles in the lower part of WLFZ is primarily due to sediment supply from upstream of the Yangtze River. The dominance of coarser magnetite/maghemite within the WLFZ of the upper reach of the TGR, from Jiangjin district to Fuling district, is due to strong water flow velocity. An increase in the concentration of nanosized fine-grained magnetic particles within the WLFZ of the middle and lower reaches of the TGR can be attributed to a combination of reduced water dynamics and intense regional soil erosion of nearby side slopes.

Conclusions Our findings indicate that the concentration and grain size of magnetic minerals exhibit spatial variations within the WLFZ of reservoirs under the influences of sediment provenance and hydrodynamics. These findings provide fundamental insights on future exploration into the crucial roles of iron-bearing magnetic minerals in the accumulation, migration, and transformation of pollutants and organic carbon within the WLFZ of reservoirs and their response to changes in sediment sources and water dynamics.

Keywords The Three Gorges Reservoir · Environmental magnetism · Cascade reservoirs · Sediment sources · The water-level fluctuation zone

1 Introduction

The construction of dams along a river channel traps large amounts of sediments within the resulting reservoirs (Cattanéo et al. 2021). This accumulation of sediment provides the material basis for the formation and evolution of the water level fluctuation zone (WLFZ) within reservoirs (Bao et al. 2015a;

Liro 2019). The WLFZ represents the primary wetlands in reservoirs (Anderson et al. 2018; Cattanéo et al. 2021). It has a range of ecological functions, including the burial and release of carbon (Keller et al. 2021; Jia et al. 2022), nutrients, and pollutants (Weber and Opp 2020; Singh et al. 2021).

Iron-bearing magnetic minerals (e.g., hematite and magnetite) in soils/sediments of WLFZ play important roles in the accumulation, migration, and transformation of pollutants (e.g., heavy metals and microplastics) and organic carbon (Dong et al. 2023; Hamdan et al. 2023). This is because they are capable of absorbing and accumulating pollutants, and rereleasing them as well when dissolution of iron minerals occurs under reducing conditions (Maher et al. 2008; Alagarsamy and Hoon 2018). Additionally, iron-bearing magnetic minerals, especially the active ones, are capable of retaining organic carbon in soils/sediments by absorption and co-precipitation with organic matters, and promoting its remineralization (Patzner et al. 2020; Dong et al. 2023). The understanding of the spatial distribution of magnetic minerals, their provenance, and water dynamics influencing their deposition within the WLFZ would provide the basis for future deeper analyses of the relationship between the sedimentation process, the deposition of magnetic minerals, and the migration and transformation processes of pollutants and organic carbon under the influences of water level fluctuations in reservoirs.

The Three Gorges Reservoir (TGR), located in the upper reach of the Yangtze River in China, is the results of the Three Gorges Dam, which is the largest hydropower project in the world. The fluctuation of water level between altitudes of 145 and 175 m in the TGR leads to the formation of the WLFZ spanning a length of 5578 km and covering an area of 348.93 km^2 (Su et al. 2017). Consequently, the WLFZ of the TGR provides an ideal example to understanding the accumulation process of magnetic minerals in the WFLZ of reservoirs.

Environmental magnetism, known for its simplicity, rapidity, non-destructiveness, and cost-effectiveness, has been widely used to investigate the category, grain size, and content of magnetic minerals (Dearing et al. 1981; Thompson and Oldfield 1986; Oldfield 1991; Maher and Thompson 1999; Liu et al. 2012). Additionally, magnetic properties of sediments are capable of indicating the provenance and sedimentation dynamics influencing the magnetic properties of sediments from lacustrine, oceanic, and riverine environments (Thompson and Oldfield 1986; Maher and Thompson 1999; Franciskovic-Bilinski et al. 2014; Ahmed and Maher 2018; Chaparro et al. 2020). Currently, there are few studies investigating the accumulation process of magnetic minerals in the WLFZ of the reservoirs and lakes by using environmental magnetism. For the TGR, Luo et al. (2013) conducted a study on the magnetic properties of suspended sediments from the Yangtze River, and Yang et al. (2023) investigated the relationship between magnetic minerals and heavy metal

pollutions within the WLFZ of the TGR. However, there are still lacks of detailed analyses of spatial distribution of magnetic mineral at different elevations and difference reaches within the WLFZ of the TGR, as well as their provenance and links to sedimentation dynamics.

In this study, we carry out measurements of environmental magnetism for sediments collected from various altitudes within the WLFZ, as well as nearby side-slope soils, at ten sites spanning from the tail to the head of the TGR (Fig. 1). We also assembled previously reported data on magnetic properties of suspended sediments in the upstream and tributaries flowing into the TGR. Additionally, we consider nearby side-slope soils and suspended sediments representing magnetic signals of potential sources for sediments in the WLFZ. Basing on results of magnetic properties of sediments from the WLFZ and potential sediment sources, we aim to understand the spatial distribution and provenance of magnetic minerals in sediments within the WLFZ of the TGR, and sedimentation dynamics influencing their deposition. This research will provide theoretical foundations for future deeper understanding of the impact of magnetic minerals on the retaining/releasing pollutants and organic carbon in the WFLZ of reservoirs under the influences of water-level fluctuations.

2 Materials and methods

2.1 Study area

The TGR extends approximately 660 km from Chongqing to Yichang in the upper reach of the Yangtze River (Fig. 1) and has a catchment area of 100,000 km^2. The TGR reaches its highest water level of 175 m (above sea level) in the dry season (from October to April), and the base level of 145 m in the wet season (from May to September). At its highest water level, the TGR has a water surface area of 1080 km^2 and a storage capacity of 39.3 billion m^3.

After the impoundment, the TGR receives approximately 70% of the sediments discharged from the upstream of the Yangtze River (Yang et al. 2018). According to the Changjiang Water Resources Commission (2003–2017), sedimentation deposition in the TGR has reached 1679 million tonnes (Mt), with an average deposition flux of approximately 111 Mt per year. Since 2013, sediment discharge into the TGR has decreased significantly by approximately 90%, primarily due to the construction of cascade reservoirs upstream of the Yangtze River (Guo et al. 2019; Yan et al. 2022).

Mesozoic purple sand shales or mudstones of the Jurassic Shaximiao Group (J2s) are distributed widely in the TGR basin and are characterized by high weathering propensity. Correspondingly, purple soil, the weathering

Fig. 1 The Geographical locations relevant to this study. Panel (**a**) shows the location of the watershed of the Yangtze River, in China, panel (**b**) presents the location of the Three Gorges Reservoir in the watershed of the Yangtze River, and panel (**c**) highlights the specific sample sites in the TGR. In panel (**b**), the distribution of main rock types in the Yangtze River watershed is depicted based on work by Yang et al. (2009). The yellow stars in panel (**b**) represent suspended samples collected in 2011, as referenced in Luo et al. (2013). The black stars in panel (**c**) correspond to the sample sites investigated in this study
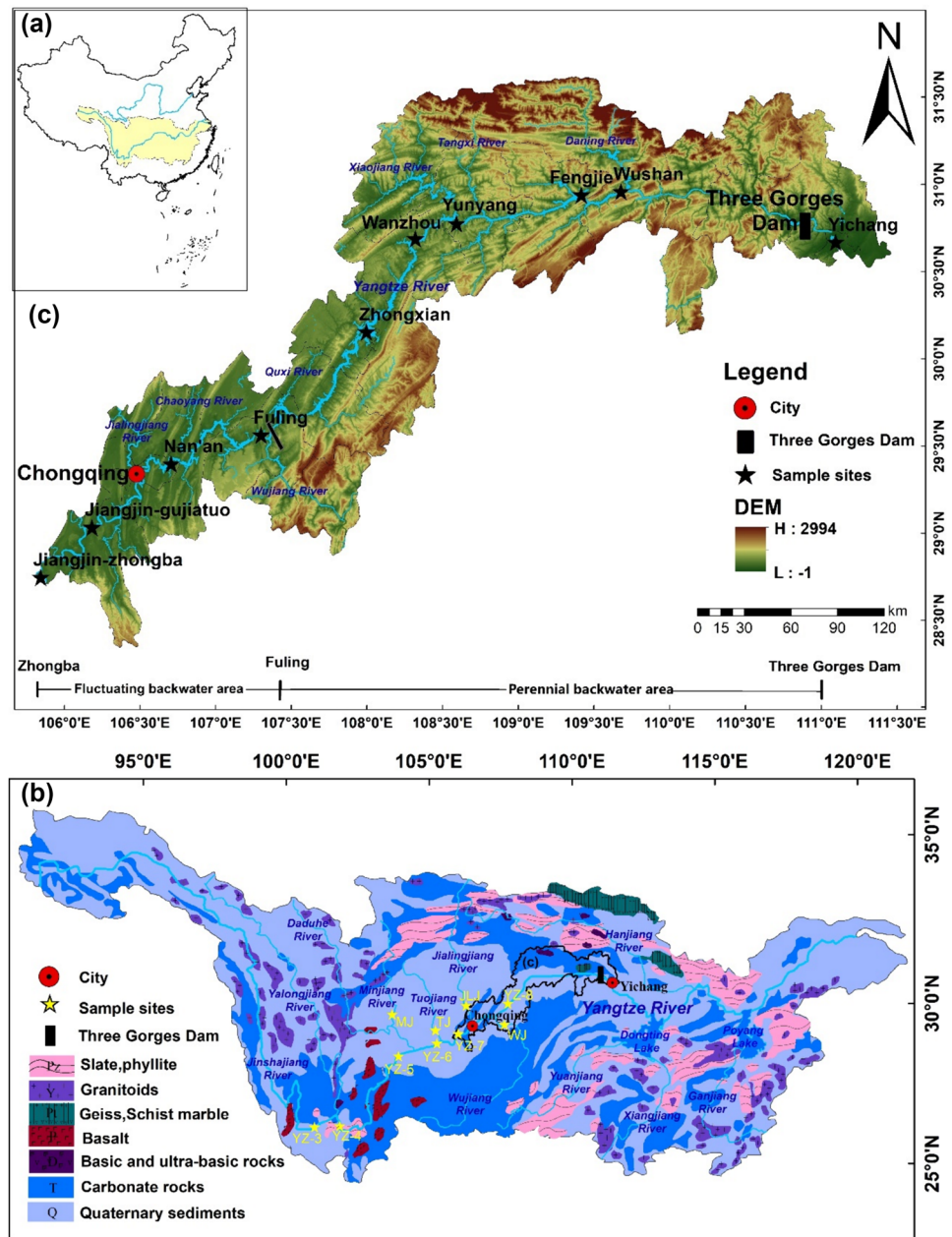
product of purple mudstones, is a dominant soil type in the study area (Wei et al. 2018). Additionally, early Triassic to Middle Triassic carbonate rocks also distribute in the TGR basin (Fig. 1b). The climate in the TGR basin is characterized by a humid subtropical monsoon climate, with an annual precipitation varying from 1100 to 1400 mm and an annual mean temperature of ~ 18 °C.

2.2 Sediment collection

In July 2018, ~ 300 sediment samples from the WLFZ and nearby side-slope soils were collected at 10 specific sites (Fig. 1 and Table 1) from the tail to the head

of the TGR by using a steel soil driller with a diameter of 3.5 cm. At the Jiangjing-Zhongba, Jiangjin-Gujiatuo, Nan'an, and Yichang sites, sediments from the WLFZ were obtained at a single elevation and labeled as submerged samples in Table 1. For the Fuling, Zhongxian, Wanzhou, Yunyang, Fengjie, and Wushan sites, sediments from the WLFZ were collected at altitudes ranging from 145–155 m, 155–165 m, and 165–175 m, respectively, wherever it is possible for sampling (Table 1). Side-slope soil samples were collected from nearby farmlands or forests located above the WLFZ and are annotated as subaerial samples or samples with altitudes higher than 175 m (> 175 m) in Table 1. At each altitude, a minimum

Table 1 Information for samples collected from the WLFZ and nearby side slopes in the TGR

The location	The Latitude and Longitude	The altitude (m)	The number of soil/sediment sections	The depths for subsample
Jiangjin-Zhongba	28°56′24.8″N, 105°51′5.7″E	submerged	3	0–30 cm
		subaerial	3	0–30 cm
Jiangjin-Gujiatuo	29°13′29.6″N, 106°11′52.64″E	submerged	3	0–20 cm
		subaerial	3	0–20 cm
Nan'an	29°35′1.87″N, 106°44′5.02″E	submerged	3	0–30 cm
		subaerial	3	0–30 cm
Fuling	29°44′19.29″N, 107°20′36.59″E	155–165	3	0–30 cm
		165–175	4	0–30 cm
		> 175	4	0–30 cm
Zhongxian	30°18′50.56″N, 108°4′29.82″E	145–155	3	0–30 cm
		155–165	4	0–30 cm
		165–175	4	0–30 cm
		> 175	3	0–30 cm
Wanzhou	30°50′24.66″N, 108°25′45.45″E	155–165	6	0–30 cm
		165–175	5	0–30 cm
		> 175	2	0–20 cm
Yunyang	30°55′5.17″N, 108°42′45.88″E	145–155	3	0–30 cm
		155–165	6	0–30 cm
		165–175	6	0–30 cm
		> 175	3	0–30 cm
Fengjie	N31°3′9.35″N, 109°34′28.14″E	145–155	2	0–30 cm
		155–165	3	0–30 cm
		165–175	6	0–30 cm
Wushan	31°3′42.37″N, 109°50′44.62″E	145–155	3	0–30 cm
		155–165	3	0–30 cm
		165–175	3	0–30 cm
		> 175	2	0–30 cm
Yichang	30°47′19.00″N, 111°8′49.68″E	submerged	3	0–30 cm
		subaerial	3	0–30 cm

of three soil or sediment sections with depths of 30 cm were randomly selected. Three subsamples were collected at depths of 0–10 cm, 10–20 cm, and 20–30 cm within each section. However, due to the thin sediment/soil layers, subsamples were only obtained at depths of 0–10 cm and 10–20 cm (Table 1) at Jiangjing-Gujiatuo site and at altitudes > 175 m at Wanzhou site. The latitudes and longitudes of the 10 WLFZ sites, the altitudes of the samples collected at each site, the number of soil or sediment sections, and the depths of subsamples within each section are provided in Table 1.

To reveal provenance of magnetic minerals in sediment within the WLFZ of the TGR, we assembled previously reported magnetic results of suspended sediment samples from various locations in the main channel of the TGR, as well as upstream regions and tributaries of the Yangtze River (Luo et al. 2013). These samples are considered as potential sources for sediments in the WLFZ. Specifically, four

samples (YD-3 to YD-7) were collected from the upstream of the Yangtze River. One suspended sediment sample (YD-8) was taken from the main stream of the TRG, as shown in Fig. 1b and Table 2. Additionally, we collected four suspended sediment samples from the tributaries of the upstream of the Yangtze River including the Jialingjiang River (sample JLJ), the WuJiang River (sample WJ), the Tuojiang River (sample TJ), and the Minjiang River (sample MJ), as depicted in Fig. 1 and Table 2 (Luo et al. 2013).

These suspended sediment samples were collected in 2011 during the flooding season between July and September (Luo et al. 2013), during which sediment discharged from the upstream contributes up to ~90% of the total sediment load into the TGR. To ensure suspended sediments were representative at each sampling location, about 100 L of water were collected at a depth of about one-quarter of the total water depth when the boat was anchored in the middle of the river. All samples were collected in the upstream of a

Table 2 The previously reported magnetic results of suspended samples collected from the upstream of the Yangtze River and its tributaries (Luo et al. 2013)

The sample location	Sample name	χ_{lf} (10^{-8}m^3 kg^{-1})	χ_{fd} %	χ_{ARM} (10^{-8}m^3 kg^{-1})	SIRM (10^{-5}Am^2 kg^{-1})	HIRM (10^{-5}Am^2 kg^{-1})	S$_{-300mT}$(%)	χ_{ARM}/SIRM (10^{-5}m A^{-1})	χ_{ARM}/χ
The Jinshajiang River	YZ-3	247.37	5.36	540.88	4174.31	91.91	97.80	12.96	2.19
	YZ-4	192.11	3.93	442.71	4954.13	81.81	98.35	8.94	2.30
	YZ-5	181.58	4.29	442.71	4128.44			10.72	2.44
The main stream of the Yangtze River from where the Minjiang River meet the Yangtze River down to the middle section of the TGR	YZ-6	192.11	4.21	421.80	4495.41	136.10	96.97	9.38	2.20
	YZ-7	189.47	4.79	452.54	4220.18	127.77	96.97	10.72	2.39
	YZ-8	176.32	5.00	425.28	3807.34	125.75	96.70	11.17	2.41
The tributaries located upstream of the Yangtze River	JLJ	60.53	5.00	107.60	963.30	90.14	90.64	11.17	1.78
	WJ	60.53	4.93	90.39	963.30	50.37	94.77	9.38	1.49
	TJ	71.05	4.43	153.31	1009.17	113.88	88.72	15.19	2.16
	MJ	44.74	4.36	67.64	504.59	27.78	94.50	13.40	1.51

boat to avoid artificial pollution. Water samples were then filtered through a 0.45 µm cellulose acetate membrane to isolate suspended sediments. Subsequently, the suspended matters on the filter membrane were rinsed into a clean beaker using ultrapure water and dried in an oven at 40 ℃.

2.3 Magnetic measurements

In this study, all samples collected from the WLFZ and side-slope soils in the TGR were naturally air-dried for magnetic measurements. These samples, as well as those reported in Luo et al. (2013), were all prepared and measured in the following standardized procedures. Specifically, about 2 g of sediments were placed in a plastic cubic box with a standard width of 2 cm. These allowed for the measurement of magnetic susceptibility, anhysteretic remanent magnetization (ARM), and isothermal remanent magnetization (IRM). For the measurement of temperature-dependent susceptibility (κ-T) curves and parameters using MicroMag 3900, the sediment samples were lightly ground using an agate mortar.

Low-frequency (976 Hz, χ_{lf}) and high-frequency (15616 Hz, χ_{lf}) magnetic susceptibility were measured using a MFK1-FA Kappa-bridge. Frequency-dependent magnetic susceptibility (χ_{fd}%) was defined as ((χ_{lf}-χ_{hf})/χ_{lf})*100 (Thompson and Oldfield 1986; Oldfield 1991). Anhysteretic remanent magnetization (ARM) was determined using a 100 mT peak alternating field with a 0.05 mT DC field superimposed, and was measured using an AGICO JR-6A spinner magnetometer. Isothermal remanent magnetization (IRM) was induced in two DC fields using an EUSCI DPM1 pulse magnetizer. Saturation isothermal remanent magnetization (SIRM) was induced at 1000 mT, and a reverse field of 300 mT (IRM$_{-300mT}$) was applied

using an EUSCI DPM1 pulse magnetizer. Remanence magnetization measured at each step was assessed using an AGICO JR-6A spinner magnetometer. S$_{-300 mT}$ was defined as (SIRM-IRM$_{-300mT}$)/(2*SIRM)*100%, while hard IRM (HIRM) was defined as (SIRM- IRM$_{-300 mT}$)/2 (Thompson and Oldfield 1986; Walden et al. 1999; Liu et al. 2012).

To provide stronger evidence for the identification of the type, grain size, and content of magnetic minerals, several representative subsamples were carefully selected for additional rock magnetic measurements. The temperature-dependent susceptibility (κ-T) curves were measured in an argon atmosphere, ranging from room temperature up to 700 °C and then back to room temperature. This was done using a MFK1-FA Kappabridge equipped with a CS-3 high-temperature furnace. Hysteresis loops, stepwise IRM, and FORC diagrams were obtained employing a MicroMag 3900 automated vibrating sample magnetometer in a maximum field of 1000 or 2000 mT (Muxworthy et al. 2002; Roberts et al. 2014). The hysteresis parameters were calculated after subtracting the paramagnetic contributions. To estimate the domain state and hence grain size of the magnetic particles, a Day plot was employed, referring to Dunlop (2002).

3 Results

3.1 Rock magnetic results and their indications of characteristics of magnetic minerals

The heating κ-T curves for representative samples obtained from the WLFZ or side-slope soils in the TGR (Fig. 2a-i) exhibit a gradual increase below ~ 200 ℃, reaching a

Fig. 2 The temperature-dependent magnetic susceptibility curves (κ-T curves) for representative samples extracted from the water-level fluctuation zone at various sites within the Three Georges Reservoir
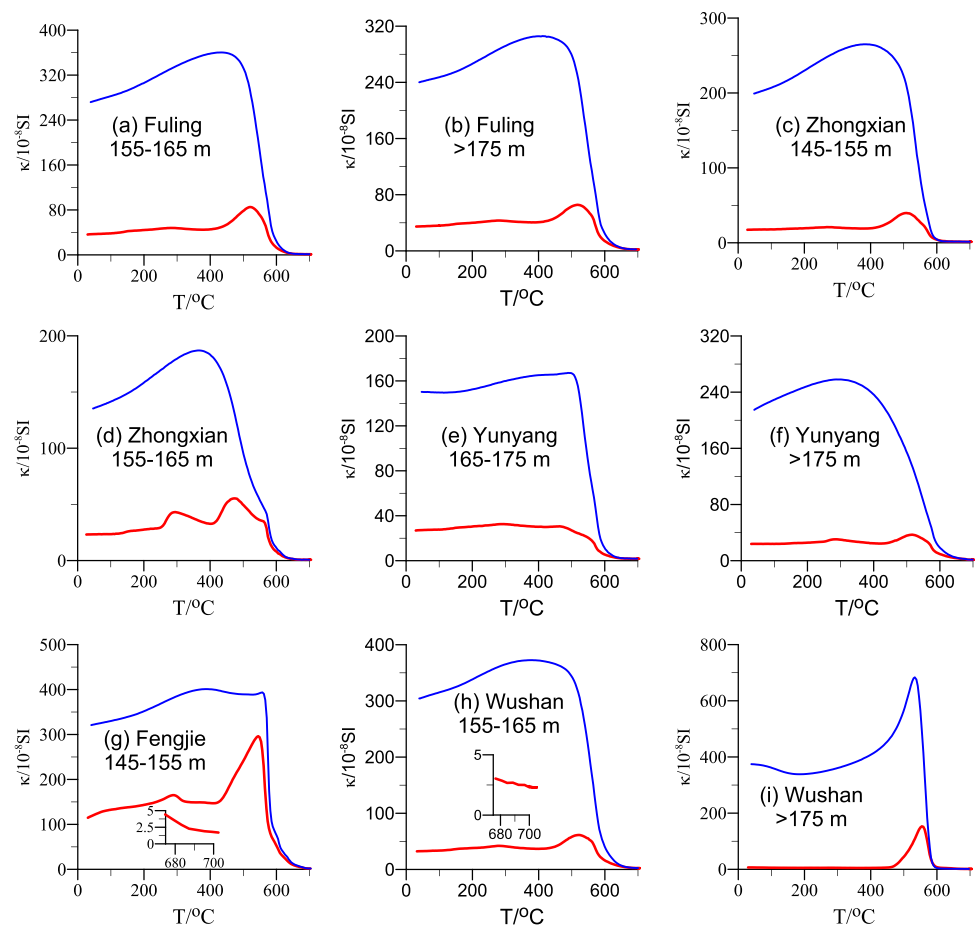

maximum around ~300 ℃. This behavior is commonly observed in samples such as Zhongxian 155–165 m (Fig. 2d) and Fengjie 145–155 m (Fig. 2g), indicating the unblocking of fine-grained magnetic particles near the superparamagnetic/single domain (SP/SD) boundary (Deng et al. 2004). The subsequent decrease in magnetic susceptibility above 300 ℃, as seen in Fig. 2d and f–h, is generally attributed to the conversion of ferrimagnetic maghemite to weakly hematite (Deng et al. 2006; Ao et al. 2010). An increase in magnetic susceptibility above ~400 ℃ is likely caused by the transformation of iron-bearing paramagnetic minerals to magnetite (Deng et al. 2006), while a rapid drop in magnetic susceptibility at around 580 ℃, representing the Curie point of magnetite, indicates the presence of magnetite.

The hysteresis loops for these representative samples (Fig. 3a-i) exhibit a rapid rise belove ~200 mT and do not fully close even at 500 mT, indicating the coexistence of low-coercivity maghemite/magnetite and high-coercivity hematite, consistent with the indications from the κ-T curves. In the case of samples Zhongxian 145–155 m (Fig. 3c), Yunyang 165–175 m (Fig. 3e), and Wushan 155–165 m (Fig. 3h), their hysteresis loops display a weak wasp-waist shape, suggesting the significant contribution of

hematite (Jiang et al. 2022). The relatively slower saturation of IRM acquisition curves and unsaturation of IRM even at 2000 mT provide further evidence for the presence of a large amount of hematite in these samples (Fig. 4a). Sample Wushan > 175 m (Fig. 3i) exhibits a typical hysteresis shape characteristic of high-coercivity hematite (Jiang et al. 2022). The very slowly acquisition of IRM and the incomplete saturation of IRM even at 2000 mT for sample Wushan > 175 m (Fig. 4a) further support the presence of a substantial amounts of hematite.

The Day-plot (Fig. 4b) analysis reveals that the magnetic minerals present in the sediments of the WLFZ and nearby side-slope soils in the TGR are primarily contributed by pseudo single-domain (PSD) particles or a mixture of single domain (SD) and multiple domain (MD) particles (Dunlop 2002). This observation is further supported by the first-order reversal curve (FORC) diagrams for these samples (Fig. 5). Their FORC diagrams exhibit a closed-contour structure in the central region, with peak B_c values ranging from 10 to 15 mT and contours spreading along the B_u axis within the range of -50 to 50 mT (Muxworthy et al. 2002; Roberts et al. 2014). For sample Fengjie 145–155 m (Fig. 5g), the presence of larger closed

Fig. 3 The hysteresis loops for typical samples taken from the water-level fluctuation zone at various sites in the Three Georges Reservoir. It should be noted that all samples have been corrected for paramagnetism
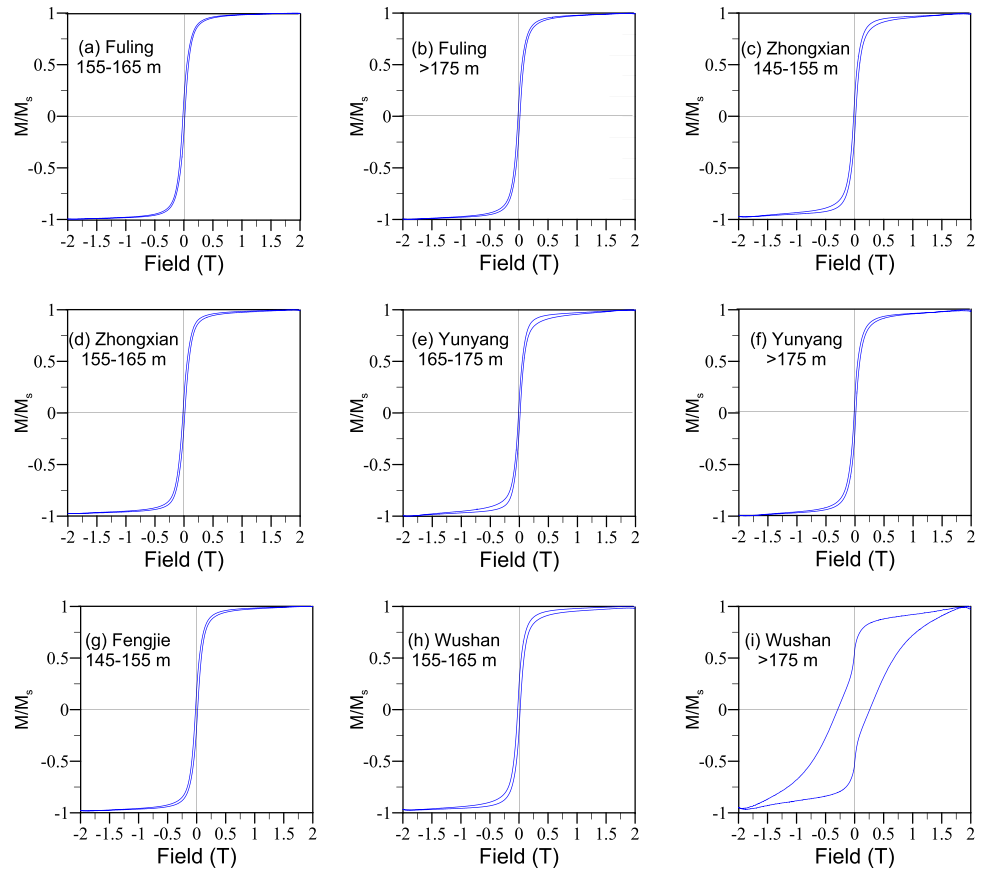

concentric contours suggests a higher contribution from fine-grained SD particles (Roberts et al. 2014), corroborating the explanations derived from the κ-T curve analysis for this particular sample. Sample Wushan > 175 m exhibits a narrow but elongated closed-contour structure

extending to ~ 140 mT on the FORC diagram (Fig. 5i), indicating the presence of typical fine-grained SD hematite (Jiang et al. 2022). This observation aligns with its location falling near the SD range on the Day-plot (Fig. 4b).

Fig. 4 The isothermal remanent magnetization (IRM) acquisition curves (**a**) and the Day plot (Dunlop 2002) of magnetic hysteresis parameters (**b**). Both panels feature representative samples collected from the water-level fluctuation zone at various sites within the Three Georges Reservoir
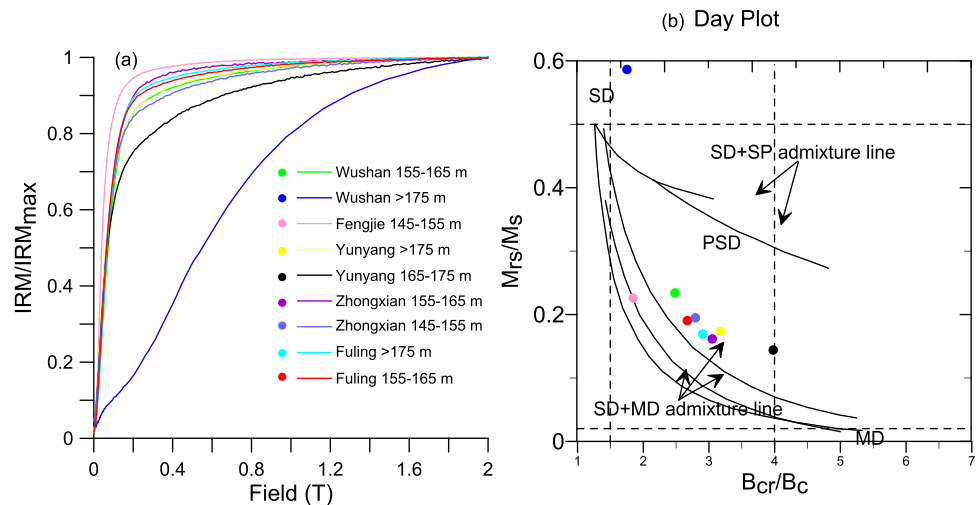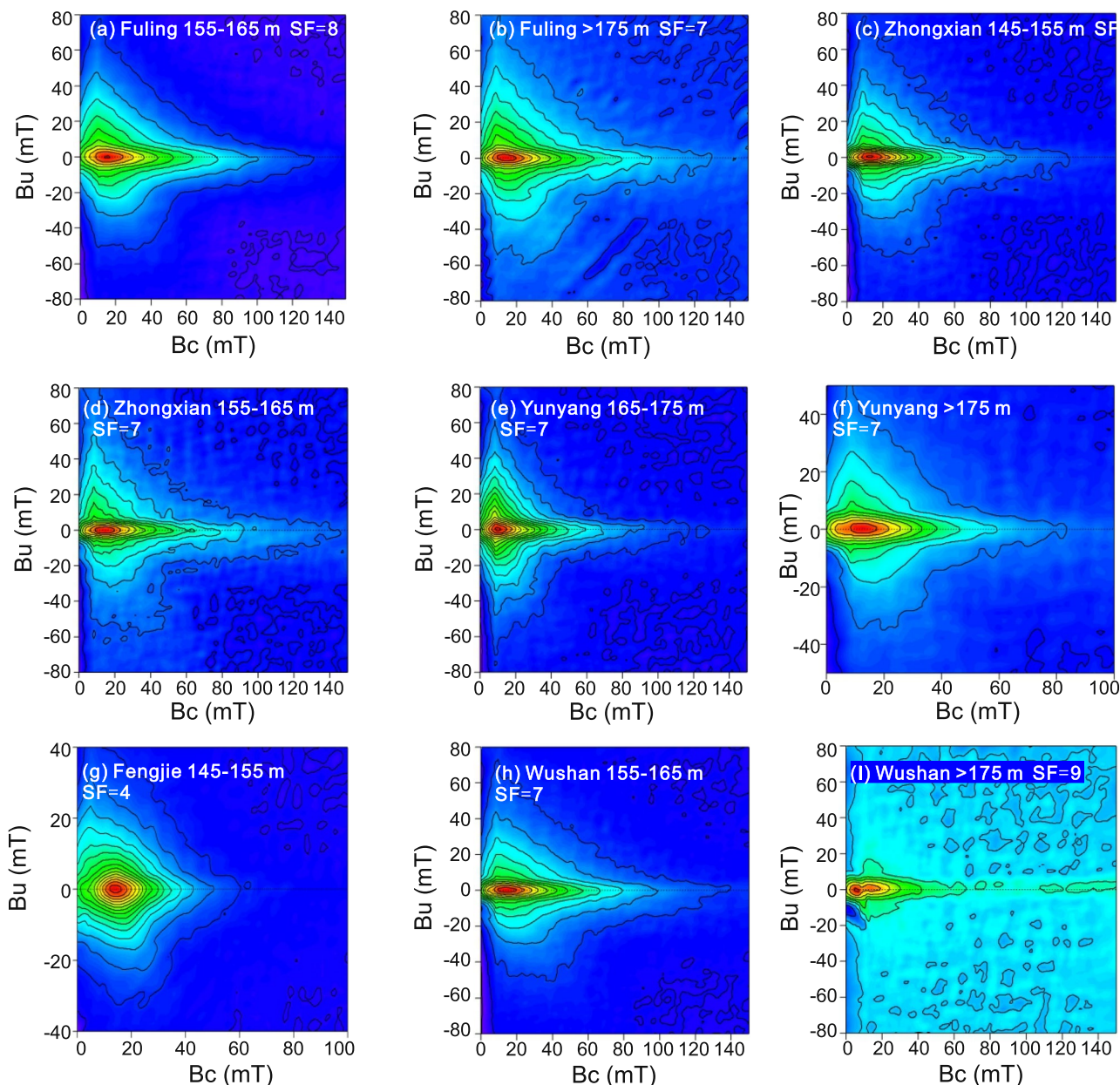
Fig. 5 The FORC diagrams for representative samples obtained from the water-level fluctuation zone at various sites within the Three Georges Reservoir

3.2 Magnetic properties for sediments from different altitude of the WLFZ and for nearby side-slope soils

In general, the magnetic parameters of samples obtained from the WLFZ exhibit similar variations to those of the adjacent side-slope soils, particularly in terms of $\chi_{fd}\%$, χ_{lf}, SIRM, and χ_{ARM}/χ_{lf}. In more detail, the sediment samples collected from the WLFZ and the nearby side-slope soils can be divided

into four sections based on the variations of magnetic parameters (Fig. 6). These sections include the Jiangjin-Zhongba to Fuling section, Zhongxian to Yunyang section, Fengjie to Wushan section, and Yichang section. The first three sections correspond to the upper reach, middle reach, and lower reach of the TGR, respectively, while the samples from Yichang are located downstream of the Three Gorges Dam.

In the upper reach (from Jiangjin-Zhongba to Fuling), both the samples from side-slope soils (samples from
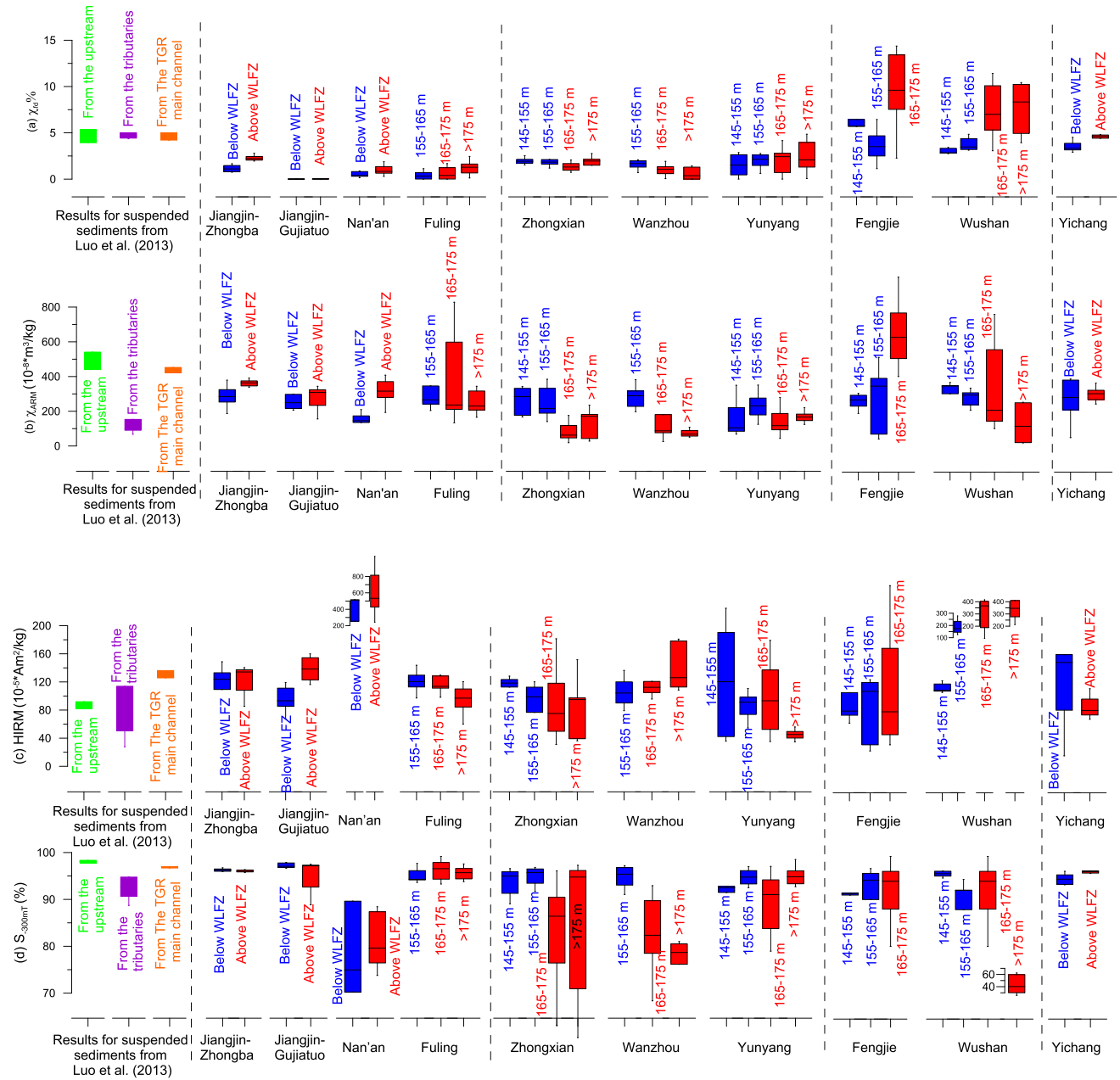
Fig. 6 The Box-whisker plots illustrating the magnetic parameters of sediment samples collected from the WLFZ and nearby side-slope soils. The blue and red colored plots represent data from this study. The green colored plots represent previously reported results of suspended samples collected from the Jinshajiang River, including samples YD-3 to YD-5 (refer to Table 4 and Fig. 1b) as documented in Luo et al. (2013). The purple colored plot represents previously reported results of suspended samples collected from tributaries located upstream of the Yangtze River, including samples MJ from

the Minjiang River, TJ from the Tuojiang River, JLJ from the Jialingjiang River, and WJ from the Wujiang River (see Table 4 and Fig. 1b) based on Luo et al. (2013). Lastly, the orange colored plot signifies samples YD-6 to YD-8 (Fig. 1b), which are suspended sediment samples taken from the main stream of the Yangtze River, specifically the section where the Minjiang River meet the Yangtze River down to the middle section of the TGR (illustrated as "the TGR main channel" in the figure) (Luo et al. 2013)
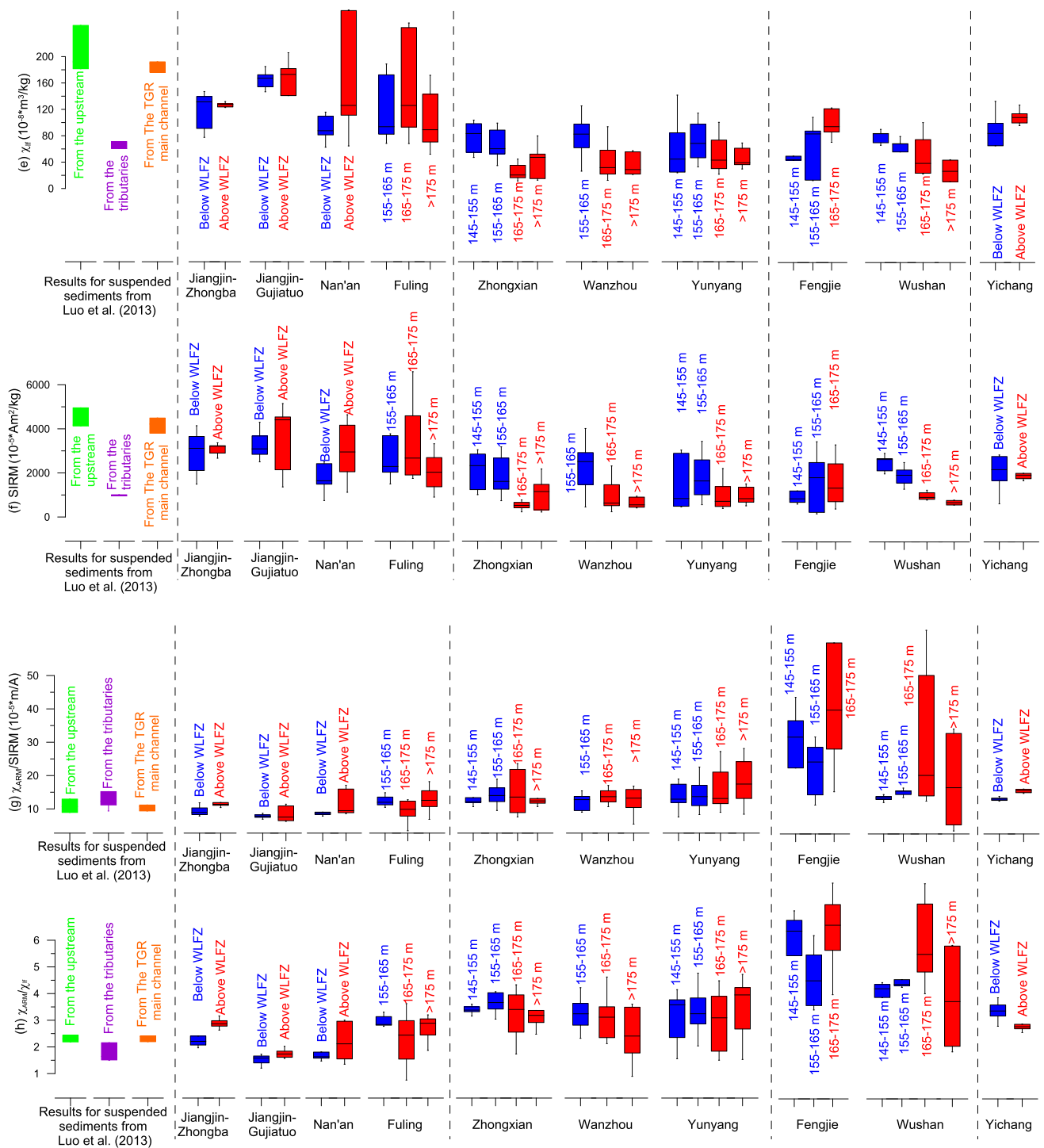
Fig. 6 (continued)

altitudes > 175 m or unsubmerged samples in Fig. 6) and the samples from the WLFZ (submerged samples and samples from altitudes < 175 m in Fig. 6) exhibit low $\chi_{fd}\%$ values, with an average of ~ 0.9% (Fig. 6a). This indicates a minimal presence of fine-grained superparamagnetic/single domain (SP/SD) particles (Maher 1988; Oldfield and Yu 1994). The

sediment from the WLFZ and the nearby side-slope soils at Nan'an display high HIRM (Fig. 6c) values and low S_{-300mT} values (Fig. 6d), with average values of $541.5*10^{-5}Am^2$ kg^{-1} and 79.9%, respectively, indicating a substantial concentration of hematite (Bloemendal et al. 1992; Walden et al. 1999). These observations align with the inferences derived

from the κ-T curves, hysteresis loops, and IRM curves for representative samples from the WLFZ. Other samples in the upper reach exhibit lower HIRM values but higher S_{-300mT} values, suggesting a relatively greater contribution of magnetite and maghemite. All samples in the upper reach display relatively high χ_{ARM} (Fig. 6b), χ_{lf} (Fig. 6e), and SIRM (Fig. 6f) values, with average values of $298.7*10^{-8}m^3\,kg^{-1}$, $128.1*10^{-8}m^3\,kg^{-1}$ and $2824.6*10^{-5}Am^2\,kg^{-1}$, respectively, further supporting the inferences of a high content of magnetite and maghemite. χ_{ARM}/SIRM (Fig. 6g) and χ_{ARM}/χ (Fig. 6h), commonly used indicators of the grain size of magnetic minerals (Liu et al. 2012), display the lowest values within the TGR, suggesting a high concentration of coarse-grained magnetic mineral particles. Comparatively, sediment from the WLFZ (submerged samples and those from altitudes lower than 165 m) exhibit lower values of $\chi_{fd}\%$, χ_{ARM}, χ_{ARM}/SIRM, and χ_{ARM}/χ than samples from the side-slope soils (unsubmerged samples and those from altitudes > 175 m). These differences indicate that the magnetic particles in sediments from the WLFZ are coarser than those in the nearby side-slope soils.

Compared to the upper reach, the HIRM values remain at a similar level for sediments from altitudes between 165–175 m of the WLFZ and side-slope soils in the middle reach from Zhongxian to Yunyang. However, the S_{-300mT} values decrease rapidly for these samples. This change pattern in HIRM and S_{-300mT} suggests a higher relative content of hematite and a lower concentration of magnetite and maghemite. The decreases in χ_{lf}, SIRM, and χ_{ARM} values further support the inference of a reduction in the concentration of magnetite and maghemite. In the middle reach, samples from altitudes of 145–155 m and 155–165 m show increased values of χ_{lf}, SIRM, χ_{ARM}, and $S_{-300\,mT}$ compared to samples at altitudes higher than 165 m, indicating an increase in the content of magnetite/maghemite. Additionally, $\chi_{fd}\%$, χ_{ARM}/SIRM and χ_{ARM}/χ values for all samples in the middle reach are larger than those for samples in the upper reach, indicating the presence of relatively finer magnetic particles in the middle reach compared to the upper reach.

For the lower reach from Fengjie to Wushan, the χ_{lf}, SIRM, HIRM and S_{-300mT} values for all samples display a similar level to those in the middle reaches, suggesting a similar composition of magnetic minerals in the middle and lower reaches. Furthermore, there is an increasing trend in the concentration of magnetite and maghemite from the upper to the lower part of the WLFZ at Site Wushan, as indicated by the increasing trends of χ_{lf}, SIRM, and S_{-300mT}, which are similar to those observed in the middle reach. In contrast, for samples at Fengjie, the content of magnetite/ maghemite displays a decreasing trend from the upper to the lower part of the WLFZ, as inferred by HIRM, χ_{lf}, SIRM and S_{-300mT}. Rapid increases in $\chi_{fd}\%$, χ_{ARM}, χ_{ARM}/SIRM and χ_{ARM}/χ values for all samples at Fengjie and Wushan

indicate a higher concentration of fine grain-sized SP and SD magnetic particles. Moreover, the content of SP/SD magnetic particles is higher for samples at altitudes higher than 165 m compared to samples at altitudes lower than 165 m.

For samples at Site Yichang, located downstream of the Three Gorges Dam, all magnetic parameters display a similar level to those in the lower reach from Fengjie to Wushan. The $\chi_{fd}\%$ and χ_{ARM}/SIRM values for submerged samples at Yichang are lower than those of unsubmerged samples, indicating a higher content of coarse-grained magnetic particles.

4 Discussions

Sedimentation hydrodynamic is a crucial factor that influences the accumulation of magnetic minerals in sediments of the WLFZ, and is primarily regulated by the strength of natural floods, the patterns of water-level fluctuations, and the morphology of the river channel, etc. (Skalak et al. 2013; Liro 2019). Sediment supply from various sources also influences the characteristics of magnetic minerals in sediments of the WLFZ (Kouhpeima et al. 2011; Pulley and Foster 2017). In this section, we firstly analyze the magnetic properties of the three potential sediment sources for the WLFZ of the TGR. Subsequently, we discuss how the magnetic properties of sediments within this zone link to sediment provenance and hydrodynamic conditions.

4.1 Magnetic property changes in different sediment sources of the WLFZ of the TGR

In analyses of sediment provenance in reservoirs, the classification of sediment sources exhibits variability, depending on the characteristics of the catchment, the sensitivity of proxies to different sources, and the availability of data, etc. (Tiecher et al. 2017; Rachels et al. 2020). In the TGR, previous studies have identified three primary of sediment sources, including the distal, the regional, and the proximal source (Wang et al. 2021a, b; Yan et al. 2022). The distal source is primarily supplied by rivers in the upper Yangtze River region, such as the Jinshajiang River, the Minjiang River, the Tuojiang River, and the Jialingjia river (Fig. 1) (Yan et al. 2022). The regional source comprises sediment contributed by adjacent tributaries of the Yangtze River within the TGR watershed, such as the Xiaojiang River and the Daninghe River (Fig. 1) (Zhou et al. 2020; Yan et al. 2022). The proximal source involves sediment derived from nearby side-slope soils due to soil erosion (Wang et al. 2021a, b).

In this study, we also categorize the provenance of magnetic minerals in sediment within the WLFZ of the TGR into the distal source, regional source, and proximal source. We propose that the nearby side-slope soils serve

as the proximal source. Additionally, the lower part of the WLFZ receives sediment contribution from the upper part of the WLFZ due to bank collapse (Bao et al. 2015b, 2018). Nearby side-slope soils collected from altitudes higher than 175 m at each site can be used to represent the magnetic properties of the original soils in the upper part of the WLFZ. This assumption is based on the similar geographic environment shared by the original soils in the upper part of the WLFZ and the side slope soils above the WLFZ prior to the impoundment of the TGR. Considering the distinct differences in magnetic properties between suspended sediments from the Jinshajiang River (a major tributary) and those from tributaries of the Yangtze River within the TGR, specifically from the point where the Minjiang River meets the Yangtze River to the head of the TGR (Fig. 1 and Table 2), we classify sediments derived from the Jinshajiang River as the distal source, and sediments derived from the tributaries of the Yangtze River within the TGR as the regional source.

Previously reported elevated values of χ_{lf}, χ_{ARM}, SIRM, and S_{-300mT} for suspended sediments from the upper Yangtze River (Fig. 1; samples YZ-3 to YZ-5 in Table 2 and green-colored samples in Fig. 6) suggest the primary presence of magnetite/maghemite (Luo et al. 2013) originating from the Fe-Ti oxide ore body of the Emeishan Large Igneous Province located near Panzhihua City, southwest of Sichuan Province (Howarth et al. 2013). The suspended sediments from the main tributaries of the Yangtze River, specifically between Minjiang and the TGR (samples JLJ, WJ, TJ, MJ in Table 2, Fig. 1 and purple samples in Fig. 6), exhibit lower concentration of magnetite/maghemite but relatively higher percentages of hematite compared to the distal source (Luo et al. 2013). These magnetic properties of the tributary sediments are attributed to the prevalence of Mesozoic purple sand shales containing abundant hematite and the yellow soils derived from early Triassic to Middle Triassic carbonate rocks in the Sichuan Basin and TGR basin (Luo et al. 2013). The main rock types in the watersheds of smaller tributaries in the TGR, such as the Daninghe River, the Xiaojiang River, and the Tangxi River, are also predominantly composed of purple sand shales and carbonate rocks. Hence, it is inferred that samples JLJ, WJ, TJ, and MJ can serve as representatives of the magnetic properties of the regional sources.

Different magnetic properties are observed for side slope soils at various sections of the TGR. In the upper reach, from Jiangjin-Zhongba to Fuling, the magnetic minerals present in side slope soils are primarily coarse magnetite/maghemite, accompanied by varying amounts of hematite, indicating the magnetic properties associated with purple sand shales and yellow soils in this region. In the middle reach, from Zhongxian to Yunyang, the magnetic minerals are characterized by a significant contribution of hematite,

as suggested by the low values of S_{-300mT}. The considerable presence of hematite suggests that side-slope soils in the middle reach primarily develop on bedrocks composed of Mesozoic purple sand shales, corresponding to the distribution of purple sand shales along the main stream of the Yangtze river in this section of the TGR (Zhong et al. 2019). In the lower reach, from Fengjie to Wushan, side slope soils exhibit abundant hematite and high concentration of fine-grained SP/SD magnetic particles, as indicated by the high values of $\chi_{fd}\%$. The presence of SP/SD magnetic particles in soils is typically attributed to the pedogenesis process (Ding et al. 2020; Ouallali et al. 2023). The high content of SP/SD particles is likely due to well-developed side-slope soils in this region, potentially influenced by the persistent high levels of forest cover in the surrounding mountainous areas (Teng et al. 2019).

4.2 The responses of magnetic minerals in sediments of WLFZ within the TGR to sediment provenance and hydrodynamics

Generally, the magnetic properties of sediments from the WLFZ exhibit a similar variation trend, to some extent, as those of side-slope soils across the upper to lower reaches of the TGR. For instance, both the sediments in the WLFZ and the adjacent side-slope soils in the upper stream display relatively higher concentration of magnetite/maghemite compared to the middle and lower reaches of the TGR, as indicated by SIRM and χ_{lf}. Similarly, both sediments in the WLFZ and side-slope soils in the middle to lower reaches of the TGR exhibit higher hematite content and slightly higher relative concentrations of fine SP/SD magnetic particles than the upper reach. These covariations of magnetic properties between sediments within the WLFZ and side-slope soils are caused by a significant contribution of side-slope soils to WLFZ. The sediment contribution from side-slope soils can be caused by intense bank or shoreline erosion induced by water wave actions of increasing backwater level during reservoir impoundment (Pal 2017; Schalko et al. 2023). Surface runoff during the drawdown period, when the banks are exposed, also contributes to bank erosion (Bao et al. 2018). Side slopes or river banks have been found to supply large percent sediments to the WLFZ in other reservoirs as well, such as Lake Winnipeg in Canada (Rodrigues et al. 2018; Goharrokhi et al. 2022).

In particular, sediments from altitudes ranging from 165 to 175 m, such as at sites Zhongxian, Wanzhou, Yunyang, and Wushan (Fig. 6), exhibit magnetic properties more similar to side-slope soils than sediments from the lower parts (from 145 to 165 m) of the WLFZ. These magnetic properties observed in the upper part of the WLFZ are likely caused by a greater contribution of sediment from side-slope soils, or by that the upper part received limited

sediment inputs from distal and regional sources and was predominantly composed of original soils. These findings align with the observations that the upper parts of the WLFZ predominantly experience sedimentation during the submersion season from October to April. This period coincides with a significant reduction in sediment discharge from the upstream of the Yangtze River and its tributaries (Tang et al. 2016, 2018). Simultaneously, bank and soil erosion at the upper part of the WLFZ are enhanced by the impact of water wave action (Bao et al. 2015a). Conversely, the lower section of the WLFZ experiences more frequent summer floods and longer flooding duration, resulting in the predominant presence of sediments originating from the Yangtze River and its tributaries (Tang et al. 2016, 2018). Compared to the WFLZ of the TGR, the absence of direct flood impacts were also used to explain sediment contributions in elevated banks of other reservoirs (Liro 2019).

In comparison, sediment samples collected from the entire WLFZ at all sites contain much lower amounts of magnetite/maghemite than suspended sediment samples collected in the Jinshajiang River (green-colored samples in Fig. 6) and suspended sediment samples in the main stream of the Yangtze River between the Minjiang River confluence and the Yangtze River to the TGR (samples YD-6, YD-7, and YD-8 in Fig. 1 and Table 2, and orange-colored sample in Fig. 6) (Luo et al. 2013), as indicated by χ_{lf}, χ_{ARM}, SIRM, and S_{-300mT}. These differences are likely caused by a significant, approximately 90%, reduction in sediment input into the TGR from the Jinshajiang River, which is known for its high content of magnetite/maghemite, since 2013, due to the construction of cascaded mega reservoirs such as Jinping-1 Reservoir, Xiangjiaba Reservoir, and Xiluodu Reservoir (Yang et al. 2018; Peng et al. 2020; Sun et al. 2021; Liu et al. 2023).

Additionally, the magnetic properties of sediments within the WLFZ exhibit distinct characteristics across different reaches of the TGR. In the upper reach, from Jiangjin to Fuling, the magnetite/maghemite particles of sediments within the WLFZ are coarser than those in the nearby side-slope soils, as well as coarser than those within the WLFZ in the middle and lower reach of the TGR, as indicated by $\chi_{fd}\%$ χ_{ARM}/SIRM and χ_{ARM}/χ. This upper reach falls within the fluctuating backwater area in the TGR (Liu et al. 2022). Coarse-grained materials transported by upstream rivers are selectively deposited within the fluctuating backwater area during periods of intense floods (Liro 2016). In the case of the TGR, the discharge of drainage water coincides with the natural flooding season from June to August (Tang et al. 2021; Liu et al. 2022). Consequently, the upper reach stretching from Jiangjin to Fuling behaves like a natural river. The resulting strong hydrodynamics induce intense riverbed erosion and sediment transport, promoting the accumulation

of coarse-grained magnetite/maghemites within the WLFZ located in the upper reaches of the TGR.

In the middle reach of the TGR, specifically from Zhongxian to Yunyang, the sediments in the lower part of the WLFZ (at altitudes between 145 and 165 m, Fig. 6) exhibit a higher abundance of magnetite/maghemite particles compared to sediments in the upper part of the WLFZ (above 165 m) and even more than sediments from the regional sources (as indicated by the purple-colored samples in Fig. 6). The middle reach of the TGR is located just within the permanent backwater area, characterized by a significantly reduction in water flow velocity (Tang et al. 2018). The decreased velocity within the permanent backwater area favors the deposition of sediments transported from the upstream during flooding season (Liro 2016, 2019; Naganna and Deka 2018). Additionally, the low-gradient of alluvial channel and the widened river valleys from Zhongxian to Yunyang facilitate sediment deposition (Steiger and Gurnell 2003; Miller et al. 2013; Ye et al. 2019). Consequently, relatively more magnetite/maghemite particles from the Jinshajiang River accumulated in the lower section of the WLFZ in this middle reach during the summer flooding season. The fining of magnetic particles in the middle reach compare to the upper reach can be attributed to rapid weakening of water flow velocity as well, combined with magnetic mineral contribution from nearby side-slope soils. This observation aligns with the longitudinal fining trend of suspended/bed sediment from the tail to the head of the TGR (Tang et al. 2018; Liu et al. 2022), and other reservoirs in the world (Liro 2016).

In the lower reach of the TGR, extending from Fengjie to Wushan, the increased contribution of fine SP/SD magnetic particles within WLFZ is primarily caused by intense soil erosion of nearby side slopes, where contain a significant amount of SP/SD particles in soils (Fig. 6). The steeper topography and higher altitudes in the lower reach of the TGR possibly contribute to this pattern (Ye et al. 2019). The slow water velocity in this typical permanent backwater area possibly plays a role as well. Additionally, a higher concentration of magnetite/maghemite particles in the lower part of the WLFZ at Site Wushan, compared its upper part, can be attributed to sediment influx from upstream regions of the Yangtze River during the summer flooding reason. This is similar to observations at Zhongxian, Wanzhou, and Yunyang. However, at Site Fengjie, the concentration of magnetite/maghemite in the lower part of the WLFZ is relatively lower compared to the upper part. This can be potentially attributed to limited sedimentation during the summer flooding season caused by steep slopes at this site. In other fluvial systems, it has also been observed that areas with higher relief and valley gradients exhibit reduced sedimentation in the riparian zone (Miller et al. 2013).

4.3 Limitations and uncertainties associated with the present study

It is important to acknowledge that there exist limitations and uncertainties in interpreting the response of magnetic properties to sediment provenance and hydrodynamics in the WLFZ in the TGR in this study. While sediment sources in the WLFZ in the TGR can be categorized as distal, regional, and proximal sources, and each exhibit distinct magnetic properties, the representation of the distal and regional sediment sources is constrained by a limited number of samples. Specifically, only three samples and four samples are available to characterize the magnetic properties of distal and regional sediment sources, respectively. More sediment samples from the distal and regional rivers would enhance the reliability of provenance analyses of magnetic minerals. Additionally, the hydrodynamic conditions in the middle to lower reaches of the TGR are weaker than the upper reaches, resulting in a higher accumulation of finer magnetic particles, such as SP/SD particles, in sediments. Correspondently, it is challenging to disentangle the respective contribution of hydrodynamic processes and the supply of fine SP/SD magnetic minerals from adjacent side slopes to magnetic properties observed within the WLFZ. We attribute the presence of finer magnetic minerals in the middle to lower reaches to a combination of both of the influx of magnetic minerals from nearby slopes and the reduced hydrodynamic forces. Despite these limitations and uncertainties, they do not significantly undermine our understanding of how magnetic minerals in the WLFZ of the TGR respond to sediment sources and hydrodynamic conditions.

5 Conclusions

This study investigates the magnetic properties of sediments collected at various elevations within the WLFZ at ten locations along the TGR, alongside exploring their provenance and the hydrodynamic conditions influencing their deposition. Our results reveal that the magnetic minerals found in the WLFZ are predominantly composed of magnetite/maghemite and hematite. Specifically, hematite particles, which mainly originated from nearby side-slopes soils, prevail in the higher elevations within the WLFZ (> 165 m) at all sites. Conversely, magnetite/maghemite particles, sourced from upstream basalt in the Emeishan region, prevails in the lower section (from 145 to 165 m) of the WLFZ.

Additionally, in the upper reach of the TGR, spanning from Jiangjin to Fuling, the WLFZ predominantly contains coarse-grained magnetite/maghemite particles. This composition can be primarily attributed to the strong water flow dynamics during the summer flooding season. In the middle reach, from Zhongxian to Yunyang, there is a notable disparity in the distribution of magnetic particles between the upper and lower parts of the WLFZ. The lower part contains a greater concentration of magnetite/maghemite particles dominantly sourced from the upper Yangtze River, which is caused by significantly reduced water velocity in the middle reach. Furthermore, the decreased water velocity also contributes to the presence of finer magnetic particles in the middle reach. In the lower reach, specifically from Fengjie to Wushan, there is a much higher concentration of SP/SD particles in the sediment. The increased presence of these particles can be attributed to both side-slope soil erosions and the diminished water velocity in this area. This study provides fundamental information for future investigations of how iron-bearing magnetic minerals in mediating the transport and transformation of pollutants and organic carbon within WLFZ under the influences of changes in sediment source and hydrodynamic conditions.

Data availability The data that support the findings of this study are available from the corresponding author Ting Chen (chenting@cqnu.edu.cn) upon reasonable request.

Declarations

Conflicts of interest The authors declare that there is no conflict of interest exists in the submission of this manuscript.

References

Ahmed IAM, Maher BA (2018) Identification and paleoclimatic significance of magnetite nanoparticles in soils. PANS 115:1736–1741

Alagarsamy R, Hoon SR (2018) Metal pollutants in Indian continental coastal marine sediment along a 3700 km transect: An electron paramagnetic resonance spectroscopic study. Sci Total Environ 612:26–38

Anderson EP, Jenkins CN, Heilpern S, Maldonado-Ocampo JA, Carvajal-Vallejos FM, Encalada AC, Rivadeneira JF, Hidalgo M, Cañas CM, Ortega H, Salcedo N, Maldonado M, Tedesco PA (2018) Fragmentation of Andes-to-Amazon connectivity by hydropower dams. Sci Adv 4:eaao164

Ao H, Deng CL, Dekkers MJ, Liu QS (2010) Magnetic mineral dissolution in Pleistocene fluvio-lacustrine sediments, Nihewan Basin (North China). Earth Planet Sci Lett 292:191–200

Bao YH, Gao P, He XB (2015a) The water-level fluctuation zone of Three Gorges Reservoir A unique geomorphological unit. Earth Sci Rev 150:14–24

Bao YH, Tang Q, He XB, Hu YH, Zhang XB (2015b) Soil erosion in the riparian zone of the Three Gorges Reservoir, China. Hydrol Res 46:212–221

Bao Y, He X, Wen A, Gao P, Tang Q, Yan D, Long Y (2018) Dynamic changes of soil erosion in a typical disturbance zone of China's Three Gorges Reservoir. CATENA 169:128–139

Bloemendal J, King J, Hall F, Doh SJ (1992) Rock magnetism of Late Neogene and Pleistocene deep-sea sediments: Relationship to sediment source, diagenetic processes, and sediment lithology. JRG: SE (1978-2012) 97:4361–4375

Cattanéo F, Guillard J, Diouf S, O'Rourke J, Grimardias D (2021) Mitigation of ecological impacts on fish of large reservoir sediment management through controlled flushing - The case of the Verbois dam (Rhone River, Switzerland). Sci Total Environ 756:144503

Chaparro MAE, Ramírez-Ramírez M, Chaparro MAE, Miranda-Avilés R, Puy-Alquiza MJ, Böhnel HN, Zanor GA (2020) Magnetic parameters as proxies for anthropogenic pollution in water reservoir sediments from Mexico: An interdisciplinary approach. Sci Total Environ 700:134343

Dearing JA, Elner JK, Happey-Wood CM (1981) Recent sediment flux and erosional processes in a Welsh upland lake-catchment based on magnetic susceptibility measurements. Quat Res 16:356–372

Deng CL, Zhu RX, Verosub KL, Singer MJ, Vidic NJ (2004) Mineral magnetic properties of loess/paleosol couplets of the central loess plateau of China over the last 1.2 Myr. J Geophys Res 109:B01103

Deng CL, Shaw J, Liu QS, Pan Y, Zhu R (2006) Mineral magnetic variation of the Jingbian loess/paleosol sequence in the northern Loess Plateau of China: Implications for Quaternary development of Asian aridification and cooling. Earth Planet Sci Lett 241:248–259

Ding ZH, Zhang ZD, Li YC, Zhang LZ, Zhang KL (2020) Characteristics of magnetic susceptibility on cropland and pastureland slopes in an area influenced by both wind and water erosion and implications for soil redistribution patterns. Soil Tillage Res 199:104568

Dong H, Zeng Q, Sheng Y, Chen C, Yu G, Kappler A (2023) Coupled iron cycling and organic matter transformation across redox interfaces. Nat Rev Earth Environ 4:659–673

Dunlop DJ (2002) Theory and application of the Day plot (Mrs/Ms versus Hcr/Hc) 2. Application to data for rocks, sediments, and soils. J Geophys Res 107:2057

Franciskovic-Bilinski S, Scholger R, Bilinski H, Tibljas D (2014) Magnetic, geochemical and mineralogical properties of sediments from karstic and flysch rivers of Croatia and Slovenia. Environ Earth Sci 72:3939–3953

Goharrokhi M, McCullough GK, Lobb DA, Owens PN, Koiter AJ (2022) Sediment sources and transport dynamics in large, regulated river systems with multiple lakes and reservoirs in the subarctic region of Canada. Hydrol Processes 36:e14675

Guo L, Su N, Townend I, Wang ZB, Zhu C, Wang X, Zhang Y, He Q (2019) From the headwater to the delta: A synthesis of the basin-scale sediment load regime in the Changjiang River. Earth Sci Rev 197:102900

Hamdan A, Lubis SS, Nazla CT, Jaswita D, Maulida Z, Munandar A, Hamdi H, Ardiansyah R, Khairuzzaman H (2023) Magnetic susceptibilites of suspended sediment and microplastic abundance in a tropical volcanic estuary. Reg Stud Mar Sci 61:102927

Howarth GH, Prevec SA, Zhou MF (2013) Timing of Ti-magnetite crystallisation and silicate disequilibrium in the Panzhihua mafic layered intrusion: Implications for ore-forming processes. Lithos 170:73–89

Jia J, Gao Y, Sun K, Wang S, Wang J, Li Z, Lu Y, Deng W, Ha X (2022) Drawdown zone can shift a floodplain-lake system from a steady carbon source to an unsteady carbon sink. Agric for Meteorol 327:109224

Jiang ZX, Liu QS, Roberts AP, Dekkers MJ, Barron V, Torrent J, Li SZ (2022) The magnetic and color reflectance properties of hematite: from Earth to Mars. Rev Geophys 60:e2020RG000698

Keller PS, Marcé R, Obrador B, Koschorreck M (2021) Global carbon budget of reservoirs is overturned by the quantification of drawdown areas. Nat Geosci 14:402–408

Kouhpeima A, Feiznia S, Ahmadi H (2011) Tracing fine sediment sources in small mountain catchment. Water Sci Technol 63:2324–2330

Liro M (2016) Development of sediment slug upstream from the Czorsztyn Reservoir (southern Poland) and its interaction with river morphology. Geomorphology 253:225–238

Liro M (2019) Dam reservoir backwater as a field-scale laboratory of human-induced changes in river biogeomorphology: A review focused on gravel-bed rivers. Sci Total Environ 651:2899–2912

Liu Q, Roberts AP, Larrasoaña JC, Banerjee SK, Guyodo Y, Tauxe L, Oldfield F (2012) Environmental magnetism: principles and applications. Rev Geophys 50:RG4002

Liu SW, Li DX, Liu DC, Zhang XF, Wang ZL (2022) Characteristics of sedimentation and sediment trapping efficiency in the Three Gorges Reservoir China. Catena 208:105715

Liu J, Zheng H, Shen Y, Xing B, Wang X (2023) Variation in sediment sources and the response of suspended sediment grain size in the upper Changjiang River Basin following the large dam constructions. Sci Total Environ 904:166869

Luo C, Zheng Y, Zheng H, Wang P, He M, Wu W (2013) Magnetic properties of suspended sediment in the Yangtze river and its provenance implications. Quat Sci 33:684–696

Maher BA (1988) Magnetic properties of some synthetic sub-micron magnetites. Geophys J 94:83–96

Maher BA, Thompson R (1999) Quaternary climates, environments and magnetism. Cambridge University Press, London

Maher BA, Moore C, Matzka J (2008) Spatial variation in vehicle-derived metal pollution identified by magnetic and elemental analysis of roadside tree leaves. Atmos Environ 42:364–373

Miller JR, Mackin G, Lechler P, Lord M, Lorentz S (2013) Influence of basin connectivity on sediment source, transport, and storage within the Mkabela Basin South Africa. Hydrol Earth Syst Sci 17:761–781

Muxworthy AR, Dunlop DJJE, Letters PS (2002) First-order reversal curve (FORC) diagrams for pseudo-single-domain magnetites at high temperature. Earth Planet Sci Lett 203:369–382

Naganna SR, Deka PC (2018) Variability of streambed hydraulic conductivity in an intermittent stream reach regulated by Vented Dams: A case study. J Hydrol 562:477–491

Oldfield F (1991) Environmental magnetism-A personal perspective. Quater Sci Rev 10:73–85

Oldfield F, Yu L (1994) The influence of particle size variations on the magnetic properties of sediments from the north-eastern Irish Sea. Sedimentology 41:1093–1108

Ouallali A, Bouhsane N, Bouhlassa S, Moukhchane M, Ayoubi S, Aassoumi H (2023) Rapid magnetic susceptibility measurement as a tracer to assess the erosion–deposition process using tillage homogenization and simple proportional models: A case study in northern of Morocco. Int J Sediment Res 38:739–753

Pal S (2017) Impact of Tilpara barrage on backwater reach of Kushkarni River: a tributary of Mayurakshi River. Environ Dev Sustain 19:2115–2142

Patzner MS, Mueller CW, Malusova M, Baur M, Nikeleit V, Scholten T, Hoeschen C, Byrne JM, Borch T, Kappler A, Bryce C (2020) Iron mineral dissolution releases iron and associated organic carbon during permafrost thaw. Nat Commun 11:6329

Peng T, Tian H, Singh VP, Chen M, Liu J, Ma HB, Wang JB (2020) Quantitative assessment of drivers of sediment load reduction in the Yangtze River basin China. J Hydrol 580:124242

Pulley S, Foster I (2017) Can channel banks be the dominant source of fine sediment in a UK river?: an example using ^{137}Cs to interpret sediment yield and sediment source. Earth Surf Proc Land 42:624–634

Rachels AA, Bladon KD, Bywater-Reyes S, Hatten JA (2020) Quantifying effects of forest harvesting on sources of suspended sediment to an Oregon Coast Range headwater stream. For Ecol Manage 466:118123

Roberts AP, Heslop D, Zhao X, Pike CR (2014) Understanding fine magnetic particle systems through use of first-order reversal curve diagrams. Rev Geophys 52:557–602

Rodrigues MF, Reichert JM, Burrow RA, Flores EMM, Minella JPG, Rodrigues LA, Oliveira JSS, Cavalcante RBL (2018) Coarse and fine sediment sources in nested watersheds with eucalyptus forest. Land Degrad Dev 29:2237–2253

Schalko I, Follett E, Nepf H (2023) Impact of lateral gap on flow distribution, backwater rise, and turbulence generated by a logjam. Water Resour Res 59:e2023WR34689

Singh R, Tiwari AK, Singh GS (2021) Managing riparian zones for river health improvement: an integrated approach. Landsc Ecol Eng 17:195–223

Skalak KJ, Benthem AJ, Schenk ER, Hupp CR, Galloway JM, Nustad RA, Wiche GJ (2013) Large dams and alluvial rivers in the Anthropocene: The impacts of the Garrison and Oahe Dams on the Upper Missouri River. Anthropocene 2:51–64

Steiger J, Gurnell AM (2003) Spatial hydrogeomorphological influences on sediment and nutrient deposition inriparian zones: observations from the Garonne River, France. Geomorphology 49:1–23

Su X, Nilsson C, Pilotto F, Liu S, Shi S, Zeng B (2017) Soil erosion and deposition in the new shorelines of the Three Gorges Reservoir. Sci Total Environ 599–600:1485–1492

Sun J, Zhang F, Zhang X, Lin B, Yang Z, Yuan B, Falconer RA (2021) Severely declining suspended sediment concentration in the heavily dammed Changjiang fluvial system. Water Resour Res 57:e2021WR030370

Tang Q, Bao YH, He XB, Fu BJ, Collins AL, Zhang XB (2016) Flow regulation manipulates contemporary seasonal sedimentary dynamics in the reservoir fluctuation zone of the Three Gorges Reservoir, China. Sci Total Environ 548:410–420

Tang Q, Collins AL, Wen A, He X, Bao Y, Yan D, Long Y, Zhang Y (2018) Particle size differentiation explains flow regulation controls on sediment sorting in the water-level fluctuation zone of the Three Gorges Reservoir, China. Sci Total Environ 633:1114–1125

Tang XY, Tong SC, Huang GX, Xu GX, Li XH, Lei K, Yao SM (2021) Characteristics of sedimentation and channel adjustment linked to the Three Gorges Reservoir. Int J Sediment Res 36:177–189

Teng MJ, Huang CB, Wang PC, Zeng LX, Zhou ZX, Xiao WF, Huang ZL, Liu CF (2019) Impacts of forest restoration on soil erosion in the Three Gorges Reservoir area. China Sci Total Environ 697:134164

Thompson R, Oldfield F (1986) Environmental Magnetism. Allen and Unwin, London

Tiecher T, Minella JPG, Caner L, Evrard O, Zafar M, Capoane V, Le Gall M, dos Santos DR (2017) Quantifying land use contributions to suspended sediment in a large cultivated catchment of Southern Brazil (Guapore River, Rio Grande do Sul). Agric Ecosyst Environ 237:95–108

Walden J, Oldfield F, Smith J (1999) Environmental magnetism: a practical guide (Technical Guide 6). Quaternary research association, London, p 243

Wang S, Rao W, Qian J, Jin K, Li K, Feng Y, Zhao J (2021a) Sr-Nd isotope and REE compositions of surface sediments from the Three Gorges Reservoir: Implications for source identification and apportionment. J Hydrol 598:126279

Wang S, Rao W, Qian J, Jin K, Li K, Feng Y, Zhao J (2021b) Identifying the provenance of bottom sediments in the Three Gorges Reservoir using stable Pb isotopes. CATENA 207:105656

Weber CJ, Opp C (2020) Spatial patterns of mesoplastics and coarse microplastics in floodplain soils as resulting from land use and fluvial processes. Environ Pollut 267:115390

Wei J, Shi B, Li J, Li S, He X (2018) Shear strength of purple soil bunds under different soil water contents and dry densities: A case study in the Three Gorges Reservoir Area, China. CATENA 166:124–133

Yan HC, Zhang XF, Xu QX (2022) Unprecedented sedimentation in response to emerging cascade reservoirs in the upper Yangtze River Basin. CATENA 209:105833

Yang S, Wang Z, Guo Y, Li C, Cai J (2009) Heavy mineral compositions of the Changjiang (Yangtze River) sediments and their provenance-tracing implication. J Asian Earth Sci 35:56–65

Yang HF, Yang SL, Xu KH, Milliman JD, Wang H, Yang Z, Chen Z, Zhang CY (2018) Human impacts on sediment in the Yangtze River: A review and new perspectives. Glob Planet Change 162:8–17

Yang D, Yang X, An N, Xie ZQ (2023) Effect of land use conversion on heavy metals and magnetic minerals on water reservoir riparian soils. Chemosphere 331:138771

Ye C, Butler OM, Du M, Liu WZ, Zhang QF (2019) Spatio-temporal dynamics, drivers and potential sources of heavy metal pollution in riparian soils along a 600 kilometre stream gradient in Central China. Sci Total Environ 651:1935–1945

Zhong SQ, Han Z, Duo J, Ci E, Ni JP, Xie DT, Wei CF (2019) Relationships between the lithology of purple rocks and the pedogenesis of purple soils in the Sichuan Basin. China Sci Rep 9:13272

Zhou Y, Li D, Lu J, Yao S, Yan X, Jin Z, Liu L, Lu XX (2020) Distinguishing the multiple controls on the decreased sediment flux in the Jialing River basin of the Yangtze River Southwestern China. Catena 193:104593

Authors and Affiliations

Ting Chen[1] · Yujie Chen[1] · Xiaofeng Wang[1] · Xingping Wei[1] · Liuliu Feng[1] · Yixuan Wang[1]

✉ Xiaofeng Wang
   xiaofeng6540@163.com

[1] Chongqing Key Laboratory of Carbon Cycle and Carbon Regulation of Mountain Ecosystem, Chongqing Normal University, Chongqing 401331, People's Republic of China